Photochemical & Photobiological Sciences
https://doi.org/10.1007/s43630-021-00074-2

ORIGINAL PAPERS

Amphiphilic tricationic Zn(II)phthalocyanine provides effective photodynamic action to eradicate broad-spectrum microorganisms

Estefanía Baigorria[1] · Javier E. Durantini[2] · María A. Di Palma[1] · Natalia S. Gsponer[1] · María E. Milanesio[1] · Edgardo N. Durantini[1]

Received: 26 April 2021 / Accepted: 5 July 2021

Abstract

A novel tricationic Zn(II)phthalocyanine derivative, $(NCH_3)_3ZnPc^{3+}$, was synthesized by ring expansion reaction of boron(III) [2,9(10),16(17)-trinitrosubphthalocyaninato]chloride. First, the reaction of this subphthalocyanine with 2,3-naphthalenedicarbonitrile and $Zn(CH_3COO)_2$ catalyzed by 8-diazabicyclo[5.4.0]undec-7-ene was used to obtain the A_3B-type nitrophthalocyanine. After reduction of nitro groups with Na_2S and exhaustive methylation of amino groups, $(NCH_3)_3ZnPc^{3+}$ was formed in good yields. In addition, the tetracationic analog $(NCH_3)_4ZnPc^{4+}$ was synthesized to compare their properties. The absorption and fluorescence spectra showed the Q-bands and the red emission, respectively, which are characteristic of the Zn(II)phthalocyanine derivatives in *N*,*N*-dimethylformamide. Furthermore, photodynamic activity sensitized by these compounds was studied in the presence of different molecular probes to sense the formation of reactive oxygen species. $(NCH_3)_3ZnPc^{3+}$ efficiently produced singlet molecular oxygen and also it sensitized the formation of superoxide anion radical in the presence of NADH, while the photodynamic activity of $(NCH_3)_4ZnPc^{4+}$ was very poor, possibly due to the partial formation of aggregates. Furthermore, the decomposition of L-tryptophan induced by $(NCH_3)_3ZnPc^{3+}$ was mainly mediated by a type II mechanism. Antimicrobial photodynamic inactivation sensitized by these phthalocyanines was evaluated in *Staphylococcus aureus*, *Escherichia coli*, and *Candida albicans*, as representative microbial cells. In cell suspensions, $(NCH_3)_3ZnPc^{3+}$ was rapidly bound to microbial cells, showing bioimages with red fluorescence emission. After 5 min of irradiation with visible light, $(NCH_3)_3ZnPc^{3+}$ was able to completely eliminate *S. aureus*, *E. coli* and *C. albicans*, using 1.0, 2.5 and 5.0 μM phthalocyanine, respectively. In contrast, a low photoinactivation activity was found with $(NCH_3)_4ZnPc^{4+}$ as a photosensitizer. Therefore, the amphiphilic tricationic phthalocyanine $(NCH_3)_3ZnPc^{3+}$ is a promising photosensitizing structure for application as a broad-spectrum antimicrobial phototherapeutic agent.

Keywords Phthalocyanine · Photodynamic inactivation · Reactive oxygen species · Photoinactivation · Microorganism

1 Introduction

In recent years, various events worldwide, such as natural disasters and armed conflicts, have resulted in outbreaks of numerous diseases and other public health emergencies in the world [1, 2]. Infectious diseases caused by microorganisms are part of this large number of emerging ailments. In this sense, the reduction of infectious illnesses presents a major challenge for the field of scientific research [3–5]. Since the Penicillin discovery for Fleming in 1928, chemical substances of natural and synthetic origin have been used to reduce diseases caused by microbes [6]. However, the abuse in the use of the antimicrobial substances in humans, animals, among numerous other factors, has triggered the emergence of resistance by microorganisms to such treatments

✉ Edgardo N. Durantini
edurantini@exa.unrc.edu.ar

[1] IDAS-CONICET, Departamento de Química, Facultad de Ciencias Exactas, Físico-Químicas y Naturales, Universidad Nacional de Río Cuarto, Ruta Nacional 36 Km 601, X5804BYA Río Cuarto, Córdoba, Argentina

[2] Departamento de Química, Facultad de Ciencias Exactas, IITEMA, Físico-Químicas y Naturales, Universidad Nacional de Río Cuarto, Ruta Nacional 36 Km 601, X5804BYA Río Cuarto, Córdoba, Argentina

Published online: 13 July 2021

[7]. Among the different proposed methodologies, photodynamic inactivation (PDI) of the microorganisms appears to be a promising alternative therapy for the treatment of these diseases [8, 9]. It involves the use of an appropriated photosensitizer (PS), which is rapidly bound to microbial cells. Irradiation with visible light under aerobic conditions leads to the formation of reactive oxygen species (ROS) that react with cellular components, causing loss of functionality and microbial inactivation. In this approach, two mechanisms of photodynamic action can occur in the cells. Thus, type I pathway mainly involves the reaction of the triplet excited state of the PS (^{3}PS*) and biomolecules by electron transfer or hydrogen-abstraction to form free-radicals. These intermediates can interact with ground state molecular oxygen ($O_2(^3\Delta^-_g)$) to yield superoxide anion radical ($O_2^{\cdot-}$), hydroxyl radical ($HO_2^{\cdot}$) and hydrogen peroxide (H_2O_2). Whereas, in the type II photoprocess the energy transfer from ^{3}PS* to $O_2(^3\Sigma^-_g)$ produces singlet molecular oxygen ($O_2(^1\Delta_g)$) [10]. Therefore, the generation of cell damage is linked to several factors, which mainly involve the interactions of ROS with biomolecules [11]. Consequently, the interaction between the PS and the microbial cell is highly relevant in PDI treatment. One of the first target cell sites is the cell envelope because it is the initial barrier that ROS must overcome to cause damage [11]. For this reason, positively charged drugs can affect the permeability of the cell membrane, which is highly organized and is the main barrier to the penetration of PSs into more sensitive intracellular regions [12].

Within the wide range of applicable PDI drugs, phthalocyanines appear as a promising family of phototherapeutic agents [13]. One of the most interesting characteristics of this family of compounds is that they are easily functionalized, allowing to synthesize PSs capable of interacting with microbial cells. The design and synthesis of new phthalocyanine derivatives for biomedical purposes is a major scientific challenge, since suitable structures should have a favorable lipophilic-hydrophilic balance [14]. However, a notorious disadvantage of this family of compounds is the low solubility of their unsubstituted derivatives in polar media. This is due to the extreme hydrophobicity of the aromatic macrocycle and its planarity, which results in high stability in the crystalline structure. The degree of solubility of the phthalocyanines increases with the addition of functional groups in the peripheral benzene rings of the macrocycle. This substitution can cause variations in the physical, chemical and electronic properties of the phthalocyanines [15]. The hydrophobicity–hydrophilicity ratio is important when considering the incorporation and intracellular localization in microorganisms. Therefore, it is convenient to vary the amphiphilic properties of the phthalocyanines by incorporating substituent groups [15]. In this sense, the phthalocyanines substituted by various cationic groups at the periphery of the macrocycle are especially interesting for biomedical applications [16].

In this work, we report the synthesis of a new tricationic Zn(II)phthalocyanine ($(NCH_3)_3ZnPc^{3+}$, Scheme 1) with a A_3B-symmetry. This phthalocyanine contains three cationic trimethylammonio groups in the periphery of the macrocycle combined with a naphthyl substituent. In addition, its analogous tetracationic Zn(II)phthalocyanine ($(NCH_3)_4ZnPc^{4+}$, Scheme 2) was obtained to compare the effect of the amphiphilic character on the molecular structure. PSs containing positive substituents have been more effective than anionic and neutral derivatives against bacteria and yeast. Cationic charges can interact with the cell envelop, weakening the permeability barrier of the outer membrane. This effect allows

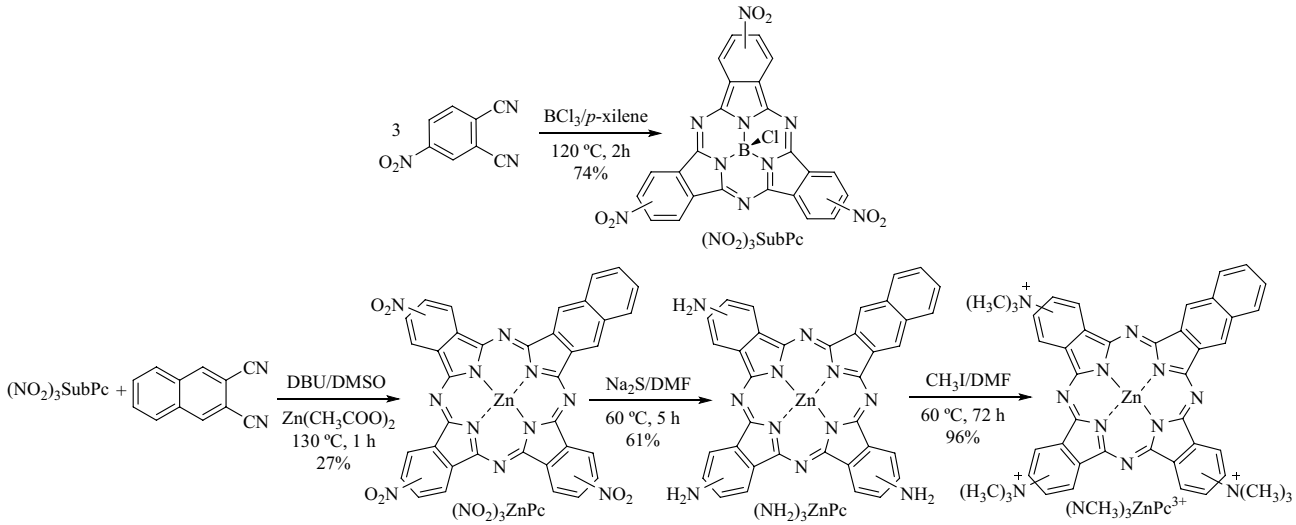

Scheme 1 Synthesis of phthalocyanine $(NCH_3)_3ZnPc^{3+}$

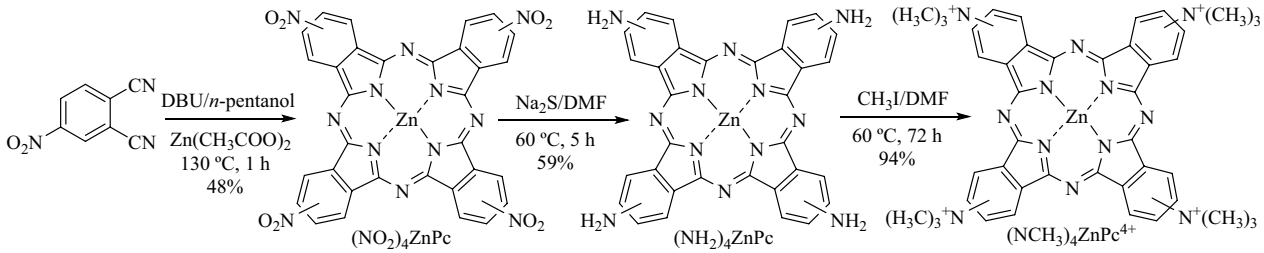

Scheme 2 Synthesis of phthalocyanine $(NCH_3)_4ZnPc^{4+}$

the penetration of cationic PSs in the most sensitive intracellular locations [8, 9]. Moreover, the spectroscopic characteristics of these PSs were studied in a homogeneous medium and the photodynamic properties were investigated to observe the formation of ROS. The photoinactivation capacities of both cationic phthalocyanines were tested in a Gram-positive bacterium *Staphylococcus aureus*, a Gram-negative bacterium *Escherichia coli*, and a yeast *Candida albicans*. These microorganisms are responsible for numerous infectious diseases that are difficult to treat in hospitals [19, 20]. Therefore, it is interesting to propose alternative therapies based on PDI for the eradication of these microbial cells.

2 Experimental section

Materials and instrumentation are specified in Supporting Information.

2.1 Synthesis of phthalocyanines

2.1.1 $(NO_2)_3$SubPc

A solution of 4-nitrophthalonitrile (515 mg, 2.97 mmol) and boron trichloride (BCl_3, 3 mmol, 3 mL of 1 M solution in *p*-xylene) was stirred at 120 °C for 2 h under an argon atmosphere. The reaction mixture was cooled to room temperature. Then, the solvent was evaporated under reduced pressure. The purple solid was purified by flash column chromatography (silica gel, toluene/ethyl acetate 10% v/v) to yield 415 mg (74%) of $(NO_2)_3$SubPc. Spectroscopic data agree with those previously reported [19, 20].

2.1.2 $(NO_2)_3$ZnPc

A solution of 2,3-naphthalenedicarbonitrile (32 mg, 0.18 mmol) and 1,8-diazabicycle[5.4.0]undec-7-ene (DBU, 12 µL, 0.12 mmol) in 2 mL of dimethylsulfoxide (DMSO) was heated to 130 °C under argon atmosphere. After that, a mixture of $(NO_2)_3$SubPc (58 mg, 0.10 mmol) and Zn(II) acetate dihydrate ($Zn(CH_3COO)_2{\cdot}2H_2O$, 26 mg, 0.12 mmol) in DMSO was added drop-wise to the heated mixture over a period of 20 min. The reaction was kept at 130 °C for 1 h. Then, the solution was cooled to room temperature and the product was precipitated with cold water (25 mL). The solid was separated by centrifugation and washed with methanol (25 mL) and cyclohexane (25 mL). The product was dried under vacuum to yield 21 mg (27%) of $(NO_2)_3$ZnPc. ^{1}HNMR (DMSO-d_6) [ppm]: 7.37–7.48 (m, 3H), 7.81–7.92 (m, 2H), 7.97–8.10 (m, 2H), 8.40–8.58 (m, 5H), 8.82–9.13 (m, 3H). FT-IR (KBr) ν (cm^{-1}): 1524 (N=O stretch), 1340 (N=O stretch), 1608 (N–H bend). ESI–MS [m/z]: 762.0581 (762.0576 calculated for $[M+H]^+$, $M=C_{36}H_{15}N_{11}O_6Zn$).

2.1.3 $(NH_2)_3$ZnPc

A solution of $(NO_2)_3$ZnPc (99 mg, 0.13 mmol) and excess of sodium sulfide nanohydrate ($Na_2S.9H_2O$, 2 g, 8.3 mmol) in 5 mL of *N,N*-dimethylformamide (DMF) was kept at 60 °C for 5 h under argon atmosphere. The reaction mixture was cooled to room temperature. The product was precipitated with cold water (25 mL). The solid was washed with water, separated by centrifugation and dried under vacuum, giving 68 mg (61%) of $(NH_2)_3$ZnPc. ^{1}HNMR (DMSO-d_6) [ppm]: 6.32 (s, 6H), 7.37–7.48 (m, 3H), 7.80–7.89 (m, 2H), 8.01–8.11 (m, 2H), 8.41–8.57 (m, 5H), 8.84–9.05 (m, 3H). FT-IR (KBr) ν (cm^{-1}): 3420 (N–H stretch), 3226 (N–H stretch), 1608 (N–H bend). ESI–MS [m/z]: 672.1357 $(M+H)^+$ (672.1351 calculated for $[M+H]^+$, $M=C_{36}H_{21}N_{11}Zn$).

2.1.4 $(NCH_3)_3ZnPc^{3+}$

A mixture of $(NH_2)_3$ZnPc (10 mg, 0.015 mmol), methyl iodide (CH_3I, 2 mL) and DMF (2 mL) was heated to 60 °C for 72 h under an argon atmosphere. The reaction mixture was cooled to room temperature. The solvent was eliminated under reduced pressure. The product was washed with cyclohexane (25 mL) and separated by centrifugation. The solid was dried under vacuum to obtain 12 mg (96%) of $(NCH_3)_3ZnPc^{3+}$. ^{1}HNMR (DMSO-d_6) [ppm]: 3.67 (s, 27H), 7.36–7.47 (m, 3H), 7.81–7.90 (m, 2H), 8.03–8.12 (m,

2H), 8.40–8.56 (m, 5H), 8.83–9.12 (m, 3H). FT-IR (KBr) ν (cm^{-1}): 3020–2822 (C–H stretch), 1660, 1460, 1417, 1261, 1016, 856. ESI–MS [m/z]: 309.3839 $[M]^{3+}$ (928.1494 calculated for $M = C_{45}H_{42}N_{11}Zn$).

2.1.5 $(NO_2)_4$ZnPc

A mixture of 4-nitrophthalonitrile (58 mg, 0.33 mmol) and $Zn(CH_3COO)_2{\cdot}2H_2O$ (30 mg, 0.14 mmol) in 5 mL of *n*-pentanol was stirred for 10 min at room temperature under argon atmosphere. Then, the mixture was treated with DBU (86 µL, 57 mmol) and refluxed for 24 h. After that, 50 mL of water was added and the product was extracted with dichloromethane (DCM, two portions of 25 mL each). The solvent was distilled under reduced pressure. The product was precipitated with *n*-heptane (25 mL) and the solid was separated by centrifugation yielding 28 mg (48%) of $(NO_2)_4$ZnPc. Spectroscopic data agree with those previously reported [21].

2.1.6 $(NH_2)_4$ZnPc

The synthesis of this compound was performed as describe above for $(NH_2)_3$ZnPc, using $(NO_2)_4$ZnPc (98 mg, 0.14 mmol) to obtain 53 mg (59%) of $(NH_2)_4$ZnPc. The spectroscopic characterization of $(NH_2)_4$ZnPc coincides with that published in the literature [21].

$(NCH_3)_4ZnPc^{4+}$. Methylation of $(NH_2)_4$ZnPc was performed as describe above for $(NCH_3)_3ZnPc^{3+}$, using $(NH_2)_4$ZnPc (10 mg, 0.016 mmol) to yield 12 mg (94%) of the pure product. Spectroscopic data coincide with those reported [22].

2.2 Computational details

Density functional theory (DFT) computations were achieved with a Gaussian 09 package (Gaussian, Wallingford, CT, USA) using the B3LYP function together with the 6-31G(d) basis set [23]. Geometries for phthalocyanines were fully optimized. Conformational searches were attained to locate the minimum-energy conformers of the structures. First, numerous geometries were formed by the conformational search modules of Spartan'14 (Wavefunction, Inc., Irvine, CA, USA) by means of MMFF force field. After that, the molecules were subjected to PM6 optimization. All structures were successively re-optimized at the B3LYP/6-31G(d) levels of theory. Molecular electrostatic potential (ESP) surfaces and molecular orbitals of the optimized structures were visualized using Avogadro Software, version 1.2.0, with an iso value of 0.007 e/au^3 and resolution of 0.10 Å [24]. The relative locations of the positive and negative charge densities in the potential surfaces were painted blue and red, respectively.

2.3 Spectroscopic studies

UV–visible absorption and fluorescence spectra of phthalocyanines were performed as reported [25]. Spectroscopic experiments were carried out in a quartz cell of 1 cm path length at room temperature. The absorbances (< 0.05) of the samples and the reference were matched at the excitation wavelength ($\lambda_{exc} = 610$ nm). The areas of the emission spectra were integrated in the range 650–800 nm. The fluorescence quantum yield (Φ_F) of phthalocyanines were calculated by comparison of the area below the corrected emission spectrum in DMF using Zn(II) 2,9(10),16(17),23(24)-tetrakis(methoxy)phthalocyanine (M_4ZnPc) as a reference ($\Phi_F = 0.26$) [26].

2.4 Photooxidation of substrates

9,10-Dimethylanthracene (DMA). Solutions of DMA (35 µM) and phthalocyanine (absorbance 0.1 at 680 nm) in DMF (2 mL) were irradiated with light at 680 nm. The decomposition of DMA after each irradiation time was determined by the decrease in the absorbance (A) at 378 nm [27]. The observed rate constants (k_{obs}^{DMA}) were obtained by a linear fit of the semilogarithmic plot of ln A_0/A *vs*. time. Under the same experimental conditions, quantum yields of $O_2(^1\Delta_g)$ production (Φ_Δ) in DMF were calculated comparing the k_{obs}^{DMA} for the corresponding PS with that obtained for M_4ZnPc, which was used as a reference ($\Phi_\Delta = 0.69$) [26].

2.4.1 Nitro blue tetrazolium (NBT)

A solution containing 0.2 mM NBT, 0.5 mM NADH and phthalocyanine (absorbance 0.1 at 680 nm) in 2 mL of DMF was used to detected $O_2^{\cdot-}$. The samples were irradiated with light at 680 nm and the progress of the reaction was observed by the increase in absorbance at 560 nm [28]. The experiments were compared with those obtained in the absence of phthalocyanine, NBT or NADH.

L-Tryptophan (Trp). Solutions of Trp (20 µM) and phthalocyanine (absorbance 0.1 at 680 nm) in 2 mL of DMF were irradiated as mentioned above for DMA. Photooxidation of Trp was analyzed by exciting the amino acid at 290 nm and determining the decrease of the fluorescence intensity (I) at 340 nm [25]. The values of k_{obs}^{Trp} were obtained by a linear fit of semilogarithmic plots of ln (I_0/I) versus time. Similarly, photooxidation of Trp sensitized by phthalocyanines was investigated in the presence of 50 mM sodium azide and 50 mM D-mannitol in DMF/water (5%).

2.5 Strains and cultures of microorganisms

The strains of microorganisms were *S. aureus* ATCC 25,923, *E. coli* EC7 and *C. albicans* PC31. These microbial cells

were previously identified and characterized [28]. Cultivation and handling of microbial cells to obtain ~ 10^8 colony-forming units (CFU)/mL for bacteria and ~ 10^6 CFU/mL for yeast in phosphate-buffered saline (PBS, pH = 7.4) were reached as described [29]. Cell viability was determined by the spread plate technique after serial dilutions tenfold in PBS. Colony formation was detected after 24 h (bacteria) or 48 h (yeast) incubation at 37 °C in the dark.

2.6 Phthalocyanine binding to microbial cells and fluorescence images

Microbial cell suspensions in PBS (2 mL) in Pyrex culture tubes (13 × 100 mm) were treated with different phthalocyanine concentrations (1.0, 2.5 and 5.0 μM) and incubation times (2, 5 and 15 min) in the dark at 37 °C. Each phthalocyanine was added from a 0.5 mM stock solution in DMF. Cells were centrifuged at 14,000 rpm for 5 min and the pellets were resuspended in 2 mL of aqueous 2% w/v SDS. The samples were kept overnight at 4 ºC and then sonicated for 30 min. The concentration of phthalocyanine in the supernatant was determined by spectrofluorimetry (λ_{exc} = 660 nm, λ_{em} = 672 nm). The fluorescence intensities of each phthalocyanine were referred to the total number of cells [30]. The concentration of the phthalocyanine in the solution was calculated by comparison with a calibration curve obtained with standard solutions (0.01–0.20 μM) of the PS in 2% w/v SDS (see Supporting Information). For microscopic images, microbial cell suspensions in PBS were treated with 5 μM $(NCH_3)_3ZnPc^{3+}$ for 30 min at 37 ºC. After being rinsed with PBS, the cells were imaged using a confocal microscope with excitation at 633 nm and emission at 640–750 nm.

2.7 Photosensitized inactivation of microorganisms

Cultures of microorganisms in PBS (2 mL) in Pyrex culture tubes (13 × 100 mm) were incubated with 1.0, 2.5 and 5.0 μM phthalocyanine for 30 min in the dark at 37 °C. Then, 200 μL of cell suspension was transferred to 96-well microtiter plates. Cultures were irradiated for different time intervals (2, 5 and 15 min for *S. aureus* and 5, 15 and 30 min for *E. coli* and *C. albicans*) with visible light at 350–800 nm of 30 mW/cm^2 (see Supporting Information) [31]. Viable cells were calculated as explained above. Each experiment was repeated three times and each value was determined in triplicate. Controls of microorganisms were carried out in the presence and absence of each phthalocyanine in the dark and in the absence of phthalocyanine with irradiated cells.

2.8 Statistical analysis

The unpaired *t* test was used to establish the significance of differences between groups. Differences between means were tested for significance by one-way ANOVA. Values were statistically significant considering a confidence level of 95% ($p < 0.05$). Data were denoted as the mean ± standard deviation of each experimental group.

3 Results and discussion

3.1 Synthesis of cationic Zn(II)phthalocyanine derivatives

The synthetic procedures to obtain $(NCH_3)_3ZnPc^{3+}$ are summarized in Scheme 1. This phthalocyanine was synthesized by four-step reactions. This approach required the formation of $(NO_2)_3$SubPc, which was synthesized by the boron trichloride-induced cyclotrimerization of 4-nitrophthalonitrile in *p*-xylene. After purification, this subphthalocyanine was obtained as a regioisomeric mixture in 74% yield. Ring expansion of $(NO_2)_3$SubPc catalyzed by DBU in the presence of 2,3-naphthalenedicarbonitrile and $Zn(CH_3COO)_2$ was performed in DMSO to obtain $(NO_2)_3ZnPc$ in 27% yield. This procedure allowed to synthesize only one phthalocyanine derivative with an A_3B-symmetry that facilitates the isolation process. Thus, this methodology has advantages over condensation of two differently substituted phthalonitriles because the statistical condensation can result in a complex mixture of phthalocyanines with different patterns of substitutions [26–34]. In previous studies, we used a similar methodology by expansion of boron(III) subphthalocyanine chloride to obtain A_3B-type phthalocyanines containing an adamantyl structure or annulations of 6-membered *N*-heterocycles with good yields [26, 32]. Reduction of nitro groups of $(NO_2)_3ZnPc$ was performed with Na_2S in DMF to yield $(NH_2)_3ZnPc$ in 61%. Finally, this aminophthalocyanine was exhaustively methylated with CH_3I in DMF to produce the tricationic $(NCH_3)_3ZnPc^{3+}$ in 96% yield.

In addition, a tetracationic analog was synthesized to compare the effect of charge distribution at the periphery of the phthalocyanine macrocycle. Scheme 2 shows the synthetic procedure to obtain $(NCH_3)_4ZnPc^{4+}$. This compound was formed from cyclotetramerization reaction of 4-nitrophthalonitrile and $Zn(CH_3COO)_2$ catalyzed by DBU in *n*-pentanol. The reaction resulted in the formation of the corresponding nitro derivative $(NO_2)_4ZnPc$ in 48% yield. This method of synthesis produced a mixture of four regioisomers with a nitro group at the 2- or 3-positions of each benzene ring in the $(NO_2)_4ZnPc$ structure [21]. The reduction of nitro groups with Na_2S was performed as described above for $(NO_2)_3ZnPc$ to yield 59% of $(NH_2)_4ZnPc$. Subsequent methylation of amino groups with CH_3I allowed to obtain the tetracationic $(NCH_3)_4ZnPc^{4+}$ in 94% yield.

The molecular structure of the PSs is primordial in the treatment of antimicrobial therapy. The positively charged

PSs present an important role in an interaction with the cell envelops [8]. The cationic phthalocyanines were optimized to a stationary point on the Born–Oppenheimer potential energy surface. Figure 1A shows the optimized structures and ESP surfaces of $(NCH_3)_3ZnPc^{3+}$ and $(NCH_3)_4ZnPc^{4+}$. The dipole moment (μ) of these cationic phthalocyanines was calculated to evaluate the effect induced by the substitution pattern on the intramolecular polarity. Values of μ = 19.52 D and μ = 0.05 D were obtained for $(NCH_3)_3ZnPc^{3+}$ and $(NCH_3)_4ZnPc^{4+}$, respectively. In the tricationic derivative, the combination of the hydrophobic naphthalene ring and hydrophilic cationic groups produces an intramolecular polarity axis. The positive charge distribution in an A_3B-symmetry significantly increases the value of μ with respect to the A_4-structure. Furthermore, spatial regions where the molecular electrostatic potential was negative and positive were determined in the molecular structure (Fig. 1B). This study allowed visualizing the charge distribution of each phthalocyanine. The positive charge in $(NCH_3)_3ZnPc^{3+}$ was mainly positioned on the cationic moiety, while the negative density was located on naphthalene ring. The amphiphilic nature of PSs can facilitate interaction with the cell envelope, generating a better accumulation in microbial cells, and therefore, increasing the photoinactivation of microorganisms.

3.2 Spectroscopic properties

The UV–visible absorption spectra of $(NCH_3)_3ZnPc^{3+}$ and $(NCH_3)_4ZnPc^{4+}$ were performed in different solvents, DMF, DCM and methanol. The spectroscopic measurements are shown in Fig. 2. The bands in the 600–700 nm region was assigned to the Q-bands transition, primarily $1a_{1u} \rightarrow 1e_g^*$ from Gouterman's 4-orbital model [35]. In DMF, the spectra of both cationic phthalocyanines showed an intense *Q*-band centered at ~ 671 nm. This band underwent a hypsochromic shift and a decrease in the intensity in methanol, while it was widened in DCM. This behavior indicates that aggregation of the cationic phthalocyanines occurred in the least polar solvent. The formation of the aggregated states generates alternatives routs of relaxation from the excited state towards the fundamental state, such as non-radiative energy dissipations. This effect produces a decrease in the formation of the ^{3}PS*, and therefore, $O_2(^1\Delta_g)$ formation, precluding the photodynamic activity [15–37]. This study confirmed that DMF is the best solvent for monomerizing the synthesized molecules. Therefore, DMF was chosen to determine the properties of the phthalocyanines in solution. Table 1 summarizes the spectroscopic properties of $(NCH_3)_3ZnPc^{3+}$ and $(NCH_3)_4ZnPc^{4+}$ in comparison with those of M_4ZnPc in DMF. The Q-bands of the cationic phthalocyanines are hypsochromically shifted with respect to that of M_4ZnPc (Figure S2). However, the shapes and the Q-band absorption maxima of $(NCH_3)_3ZnPc^{3+}$ and $(NCH_3)_4ZnPc^{4+}$ closely match the spectrum of Zn(II)phthalocyanine (ZnPc, λ_{max} = 668 nm) due to negligible auxochromic effect of the cationic trimethylammonium groups [38].

Calculations of highest occupied molecular orbital (HOMO) and lowest unoccupied molecular orbital (LUMO) of $(NCH_3)_3ZnPc^{3+}$ and $(NCH_3)_4ZnPc^{4+}$ obtained by DFT

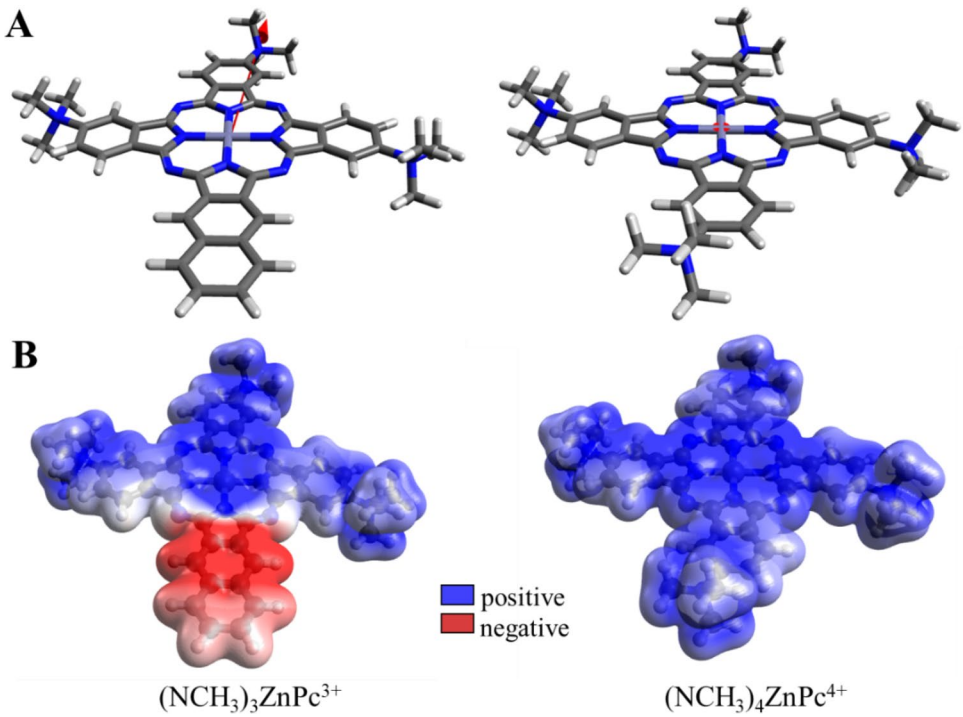

Fig. 1 **A** DFT/B3LYP/6-31G(d) optimized molecular structure and calculated relative magnitude and orientation of μ (red arrow) for $(NCH_3)_3ZnPc^{3+}$ and $(NCH_3)_4ZnPc^{4+}$, **B** ESP surfaces of cationic phthalocyanines calculated for ground state, positive (blue) and negative (red) charges.

Table 1 Spectroscopic properties of phthalocyanines and fluorescence quantum yield (Φ_F) in DMF

Phthalocyanine	λ_{max}^{abs} (nm)[a]	λ_{max}^{em} (nm)	ε (L mol^{-1} cm^{-1})[a]	Φ_F
$(NCH_3)_3ZnPc^{3+}$	671	677	1.52×10^5	0.14 ± 0.01
$(NCH_3)_4ZnPc^{4+}$	672	678	1.01×10^5	0.04 ± 0.01
M_4ZnPc[b]	676	687	2.01×10^5	0.26[b]

[a]*Q*-band, [b] from Ref. [26]

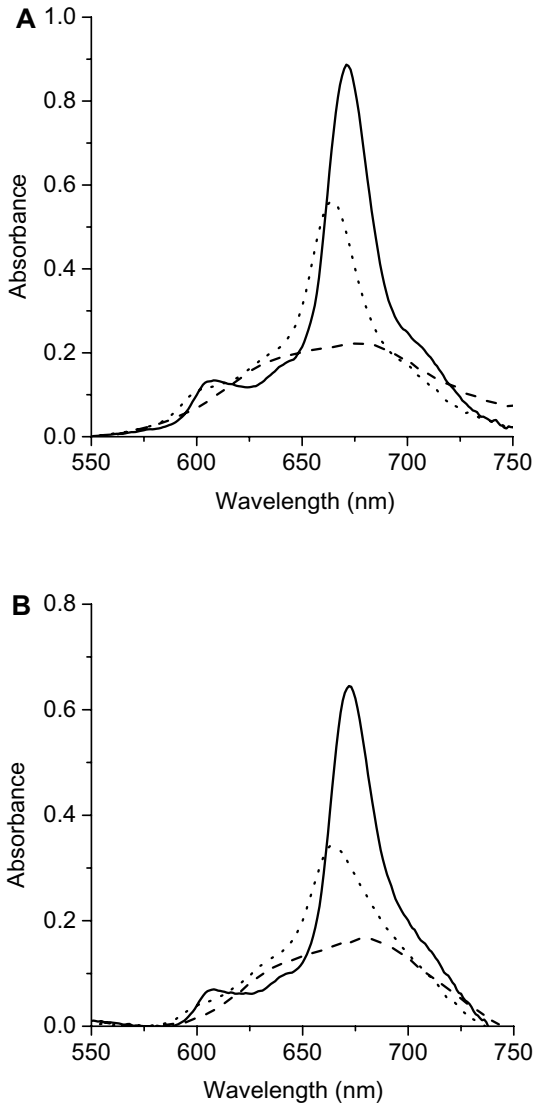

Fig. 2 Absorption spectra of **A** $(NCH_3)_3ZnPc^{3+}$ and **B** $(NCH_3)_4ZnPc^{4+}$ in different solvents: DMF (solid line), DCM (dashed line) and methanol (dotted line)

at the B3LYP/6–31 + G(d) level using Gaussian 09 are presented in Fig. 3. The HOMO of cationic phthalocyanines was formed by π orbitals localized completely on the macrocycle framework. These orbitals were regularly distributed over four isoindole rings, which were associated with the D_{4h} point symmetry of the optimized geometry for ZnPc [39]. On the other hand, the electron density in the LUMO was mainly localized on two opposite isoindole rings that coordinated to Zn atom through Zn–N bonds. As observed in the absorption results, the presence of cationic groups in the periphery of the phthalocyanine macrocycle has little effect on the distribution of the orbitals with respect to ZnPc.

The fluorescence spectra of $(NCH_3)_3ZnPc^{3+}$ and (B) $(NCH_3)_4ZnPc^{4+}$ were obtained in DMF (Fig. 4). The spectra showed two emission bands in the red, which are typical for similar Zn(II) phthalocyanine derivatives [25, 26]. For both phthalocyanines, the main emission band is centered at ~ 677 nm. The fluorescence emission and absorption spectra showed approximately mirror symmetry. The correspondence between the shape of the emission and absorption spectra in the Q-band regions indicates that the nuclear configurations of the ground and singlet excited states are similar. These emission bands correspond to Q(0–0) and Q(0–1) transitions [26]. Furthermore, the spectra of these phthalocyanines showed a small Stokes shift of 6 nm, which indicates that the spectroscopic energy is nearly identical to the relaxed energy of the singlet state and only a minor geometric relaxation occurs in the first excited state [26, 27]. The energy levels of the singlet excited states (E_s) were determined considering the energy of the 0–0 electronic transitions, giving a value of 1.84 eV for both cationic phthalocyanines, which agrees with previous results [25]. In addition, the values of Φ_F were calculated using M_4ZnPc as a reference in DMF [27]. Table 1 exhibits the results for the synthesized compounds. A higher Φ_F value was found for $(NCH_3)_3ZnPc^{3+}$ than $(NCH_3)_4ZnPc^{4+}$. This difference may be due to a partial aggregation of tetracationic phthalocyanine in DMF. The fluorescence emission of $(NCH_3)_3ZnPc^{3+}$ was adequate for the detection and quantification of this PS in microbial cells.

3.3 Photodynamic properties

Photooxidation of DMA sensitized by $(NCH_3)_3ZnPc^{3+}$ and $(NCH_3)_4ZnPc^{4+}$ was studied irradiating the samples with light at 680 nm in DMF under aerobic conditions. This substrate was used to evaluate the ability of the phthalocyanines to produce $O_2(^1\Delta_g)$. In addition, the DMA reaction was assessed in the presence of M_4ZnPc, which was used as a reference [27]. The presence of $O_2(^1\Delta_g)$ produces the oxidation of the double bonds of the central ring of the DMA forming

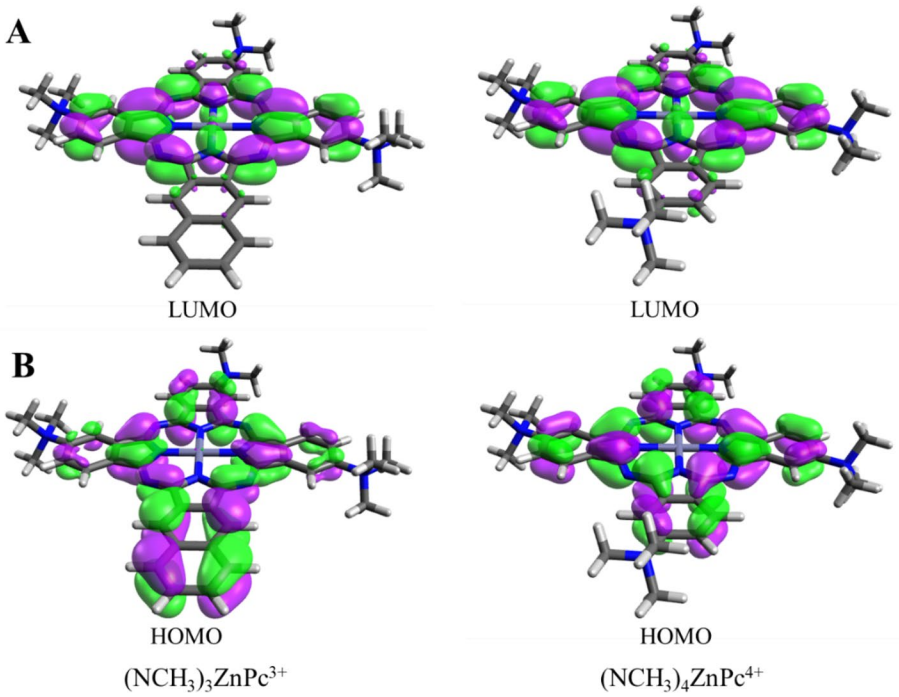

Fig. 3 **A** HOMO and **B** LUMO of $(NCH_3)_3ZnPc^{3+}$ and **B** $(NCH_3)_4ZnPc^{4+}$. Calculations were performed by DFT at the B3LYP/6–31 + G(d) level using Gaussian 09

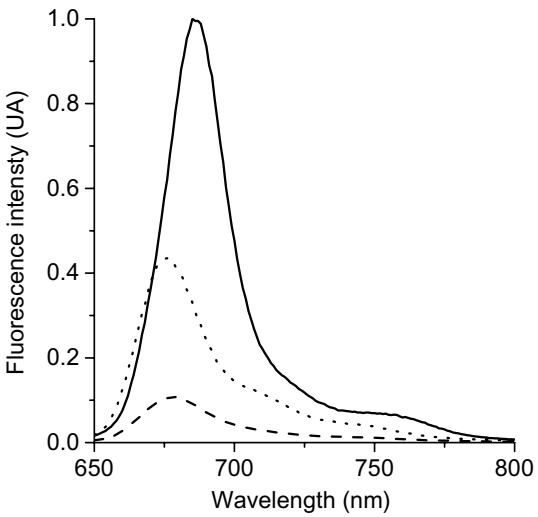

Fig. 4 Fluorescence emission spectra of $(NCH_3)_3ZnPc^{3+}$ (dotted line), $(NCH_3)_4ZnPc^{4+}$ (dashed line) and M_4ZnPc (solid line) in DMF; $\lambda_{exc} = 610$ nm

the corresponding endoperoxide. The decomposition of this subtract was observed by absorption spectroscopic measures of the band decrease at 378 nm (Figure S3). During these studies, no photobleaching of the phthalocyanines was observed. Figure 5 shows the kinetics of the DMA photooxidation sensitized by $(NCH_3)_3ZnPc^{3+}$, $(NCH_3)_4ZnPc^{4+}$ and M_4ZnPc. The values of k_{obs}^{DMA} are gathered in Table 2. In this medium, the rate of DMA decomposition sensitized by the tricationic phthalocyanine was 1.5 times slower than that produced by M_4ZnPc. In contrast, the photooxidation of DMA was very slow for $(NCH_3)_4ZnPc^{4+}$, possibly due to the formation of aggregates that preclude photodynamic action [37]. Since DMA mainly quenches $O_2(^1\Delta_g)$ by chemical reaction, the kinetic data were used to determine the values of Φ_Δ. Table 2 shows the results of Φ_Δ that were calculated comparing the k_{obs}^{DMA} for the corresponding cationic phthalocyanine with that for M_4ZnPc as a reference. As can be observed, $(NCH_3)_3ZnPc^{3+}$ was efficient to produce $O_2(^1\Delta_g)$ in DMF. Similar values of Φ_Δ were reported for a dicationic amphiphilic phthalocyanine and a tetracationic zinc(II) tetramethyltetrapyridino[3,4-*b*:3′,4′-*g*: 3″,4″-*l*: 3‴,4‴-*q*]porphyrazinium [32, 40]. However, the Φ_Δ sensitized by $(NCH_3)_4ZnPc^{4+}$ was very low as a consequence of

Table 2 Kinetic parameters (k_{obs}) for the photooxidation reaction of substrates and quantum yield of $O_2(^1_g)$ production (Φ_Δ) of phthalocyanines in DMF

Phthalocyanine	k_{obs}^{DMA} (s^{-1})	Φ_Δ	k_{obs}^{Trp} (s^{-1})[a]
$(NCH_3)_3ZnPc^{3+}$	$(5.72 \pm 0.06) \times 10^{-5}$	0.48 ± 0.05	$(3.31 \pm 0.05) \times 10^{-5}$
$(NCH_3)_4ZnPc^{4+}$	$(0.33 \pm 0.01) \times 10^{-5}$	0.02 ± 0.01	$(1.28 \pm 0.05) \times 10^{-5}$
M_4ZnPc[b]	$(8.70 \pm 0.07) \times 10^{-5}$	0.69[b]	$(4.69 \pm 0.06) \times 10^{-5}$

[a]From Ref. [26]

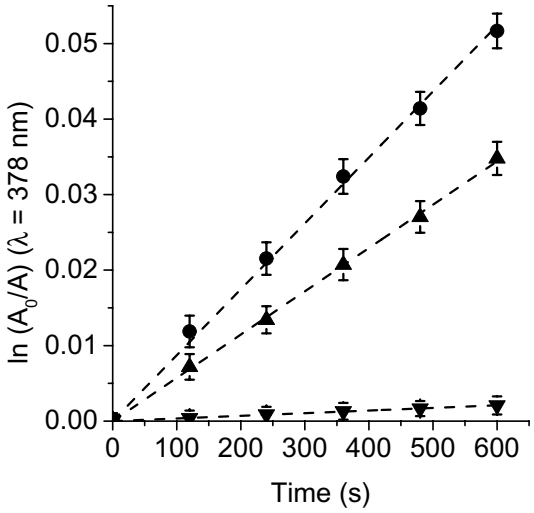

Fig. 5 First-order plots for the photooxidation of DMA (30 μM) photosensitized by $(NCH_3)_3ZnPc^{3+}$ (filled triangle), $(NCH_3)_4ZnPc^{4+}$ (inverted filled triangle) and M_4ZnPc (filled circle) in DMF; $\lambda_{irr} = 680$ nm

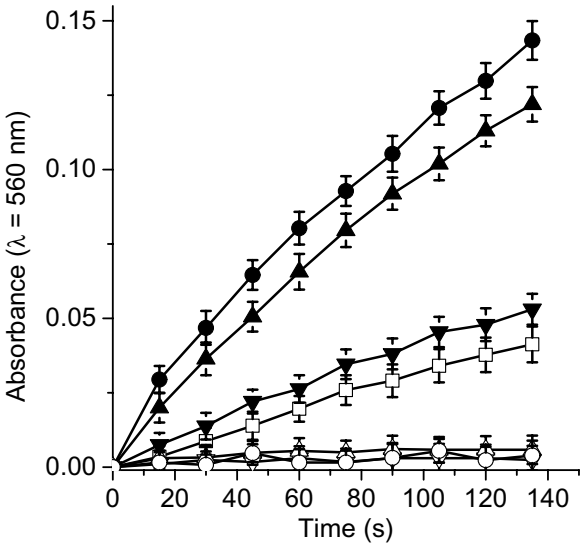

Fig. 6 Formation of $O_2^{\cdot-}$ detected by the NBT approach as an increase in the absorption at 560 nm for NBT + NADH + $(NCH_3)_3ZnPc^{3+}$ (filled triangle), NBT + NADH + $(NCH_3)_4ZnPc^{4+}$ (filled inverted triangle), NBT + NADH + M_4ZnPc (filled circle), NBT + $(NCH_3)_3ZnPc^{3+}$ (open triangle), NADH + $(NCH_3)_4ZnPc^{4+}$ (inverted open triangle), NADH + M_4ZnPc (open circle), and NBT + NADH (open square) in DMF. [NBT] = 0.2 mM and [NADH] = 0.5 mM; $\lambda_{irr} = 680$ nm

its partial aggregation in this medium [37, 41]. However, the photophysics of the phthalocyanines established in solution can significantly change in the microbial suspensions. These properties depend on the interaction of the PS with the cells and on the polarity of the intracellular microenvironment where the PS is placed. Therefore, it is difficult to predict the photodynamic behavior of phthalocyanines in cells based exclusively on photophysical studies in homogeneous media.

Moreover, the ability of $(NCH_3)_3ZnPc^{3+}$, $(NCH_3)_4ZnPc^{4+}$ and M_4ZnPc to produce $O_2^{\cdot-}$ by type I mechanism was investigated in DMF. For this purpose, phthalocyanine in the presence of NBT and the reducing agent NADH were irradiated with light at 680 nm under aerobic conditions. The reaction of NBT with $O_2^{\cdot-}$ produced formazan, which can be monitored following the absorption band of the product that was centered around 560 nm [28]. The formation of $O_2^{\cdot-}$ detected by the NBT approach is shown in Fig. 6. These results indicate that $(NCH_3)_3ZnPc^{3+}$ and M_4ZnPc produce $O_2^{\cdot-}$ when the solutions contain an electron donor agent, such as NADH. Therefore, even though these PSs form $O_2(^1\Delta_g)$ in solution, they were also capable of sensitizing the formation of $O_2^{\cdot-}$ with the addition of NADH [42]. In contrast, $(NCH_3)_4ZnPc^{4+}$ was ineffective to sensitize the formation of this ROS. In this system, phthalocyanines can be reduced to radical anion in the presence of NADH by electron transfer. From this radical anion or $^3PS^*$, phthalocyanines can transfer an electron to $O_2(^3\Sigma^-_g)$ forming $O_2^{\cdot-}$. In contrast to $O_2(^1\Delta_g)$ generation, the electron transfer type of reaction preferentially occurs in polar solvents, mainly with the incidence of the reducing agent NADH [43]. Both processes that yield $O_2(^1\Delta_g)$ and $O_2^{\cdot-}$ can be considered comparable to the main photochemical type II and type I mechanisms, respectively. However, the main cytotoxic effect in the PDI of microorganisms comes from the PS that is bound to the cells. Therefore, it is very difficult to be able to make a direct extrapolation of the photodynamic properties obtained in solution to the processes that take place in the microbial cells. The mechanisms may depend mainly on the nature of the PS, the polarity of the microenvironment where it is located into the cells, and the substrates that are in the vicinity of the PS [43–45].

Among the amino acid residues, Trp is one of the compounds most susceptible to oxidation in proteins [46]. It can be a potential target of the ROS produced by PSs in microbial environments. Trp can react with ROS to produce a complex mix of various intermediates and end-products [47]. Therefore, the photosensitized decomposition of Trp can involve ether type I or type II pathways. Photooxidation of Trp sensitized by $(NCH_3)_3ZnPc^{3+}$, $(NCH_3)_4ZnPc^{4+}$ and M_4ZnPc was studied under aerobic conditions, irradiating the solutions at 680 nm for different times. Figure 7 shows the kinetics of Trp photooxidation sensitized by phthalocyanines in DMF, following the decrease in the emission intensity at 340 nm. The values of k_{obs} for Trp decomposition are shown in Table 2. Compounds $(NCH_3)_3ZnPc^{3+}$ and M_4ZnPc showed a high production of the $O_2(^1\Delta_g)$ and they also are efficient to sensitize Trp decomposition, giving a k_{obs} considerably higher than that found for $(NCH_3)_4ZnPc^{4+}$.

Since the experimental conditions used in the decomposition of Trp were the same as for DMA and considering a type II mechanism, the reaction constant (of Trp decomposition $k_r^{Trp} = k_{obs}^{Trp}\, k_r^{DMA}/k_{obs}^{DMA}$) was calculated considering a value of $k_r^{DMA} = 5 \times 10^7\ M^{-1}\ s^{-1}$ [48]. Values of $k_r^{Trp} = (2.9 \pm 0.3) \times 10^7\ M^{-1}\ s^{-1}$ and $(2.7 \pm 0.3) \times 10^7\ M^{-1}\ s^{-1}$ were obtained for the reaction sensitized by $(NCH_3)_3ZnPc^{3+}$ and M_4ZnPc, respectively. These results are very similar to that found for the photooxidation of Trp mediated by a type II mechanism in DMF [49]. Therefore, these results showed that a type II mechanism is mainly involved for photodegradation of the substrate [50]. In addition, to obtain more evidence about the photodynamic mechanism, Trp decomposition mediated by $(NCH_3)_3ZnPc^{3+}$ and M_4ZnPc was investigated in the presence of sodium azide and D-mannitol. First, the photodynamic activity on the Trp oxidation was evaluated in the presence of sodium azide (50 mM) in DMF/water (5%) (Fig. S4). Azide ion was used as a quencher of $O_2(^1\Delta_g)$ [50]. Likewise, this substance can deactivate $^3PS^*$ through an energy transfer. A considerably reduction (3 times) in k_{obs}^{Trp} values was found for the Trp reaction sensitized by $(NCH_3)_3ZnPc^{3+}$ or M_4ZnPc in the presence of sodium azide (Table 3). Furthermore, the photosensitized decomposition of Trp was examined in the presence of D-mannitol (50 mM) in DMF/water (5%) (Fig. S4). This substrate was used as a radical scavenger, which can be formed through the incidence of type I pathway [44, 51]. For both phthalocyanines, the addition of D-mannitol induced a decrease of about 1.3 times in the reaction rates of Trp decomposition (Table 3). The results show that in the presence of the sodium azide there is a considerable decrease in the rate of photooxidation of Trp, while the protective effect was very low with the addition of D-mannitol. Therefore, these phthalocyanines decomposed the amino acid by a mechanism that involves a significant contribution of $O_2(^1\Delta_g)$.

3.4 Binding of phthalocyanine to microbial cells and fluorescence images

The ability of $(NCH_3)_3ZnPc^{3+}$ to bind to *S. aureus, E. coli,* and *C. albicans* was determined in cell suspensions (~ 10^8 CFU/mL for bacteria and ~ 10^6 CFU/mL for *C. albicans*) in PBS. For this purpose, microbial cells were incubated with 1.0, 2.5 and 5.0 µM $(NCH_3)_3ZnPc^{3+}$ for different times at 37 °C in the dark. The amount of phthalocyanine recovered after each incubation period is shown in Fig. 8. As can be observed, the PS was quickly linked to the microbial cells (2 min). An increase in the amount of $(NCH_3)_3ZnPc^{3+}$ bound to *S. aureus, E. coli,* and *C. albicans* cells was not observed prolonging the incubation times. Under this condition, the binding of $(NCH_3)_3ZnPc^{3+}$ reached values of 0.005, 0.015 and 0.029 nmol/10^8 cells for *S. aureus,* 0.003, 0.013 and 0.025 nmol/10^8 cells for *E. coli* and 0.27, 0.47 and 0.91 nmol/10^6 cells for *C. albicans* incubated with 1.0, 2.5 and 5.0 µM phthalocyanine, respectively. An increase in the uptake of $(NCH_3)_3ZnPc^{3+}$ by microbial cells was found with the PS concentrations. Consequently, non-saturation in the intracellular amount of phthalocyanine occurred, at least over this concentration range. Similar behavior was found for Zn(II) 2,9,16,23-tetrakis[4-(*N*-methylpyridyloxy)] phthalocyanine in *C. albicans* [30].

On the other hand, the cellular localization of $(NCH_3)_3ZnPc^{3+}$ in microbial cells was investigated by fluorescence confocal microscopy. Images showed that *S. aureus* (Fig. 9a) and *E. coli* (Fig. 9b) cells incubated with 5 µM PS in PBS for 30 min in the dark exhibited red fluorescence typical of phthalocyanine emission. However, the intracellular localization of PS in *E. coli* and *S. aureus* cells was

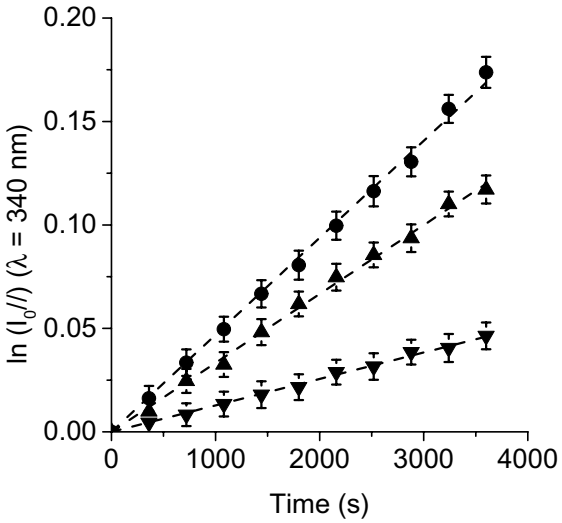

Fig. 7 First-order plots for the photooxidation of Trp (20 µM) photosensitized by $(NCH_3)_3ZnPc^{3+}$ (filled triangle), $(NCH_3)_4ZnPc^{4+}$ (inverted filled triangle) and M_4ZnPc (filled circle) in DMF; $\lambda_{irr} = 680$ nm

Table 3 Kinetic parameters (k_{obs}^{Trp}) for the photodecomposition of Trp sensitized by phthalocyanines in the presence of sodium azide (50 mM) or D-mannitol (50 mM) in DMF/water (5%)

Phthalocyanine	k_{obs}^{Trp} (s^{-1})	$k_{obs}^{Trp+azide}$ (s^{-1})	$k_{obs}^{Trp+mannitol}$ (s^{-1})
$(NCH_3)_3ZnPc^{3+}$	$(1.78 \pm 0.05) \times 10^{-5}$	$(0.61 \pm 0.02) \times 10^{-5}$	$(1.35 \pm 0.04) \times 10^{-5}$
M_4ZnPc^b	$(2.51 \pm 0.07) \times 10^{-5}$	$(0.81 \pm 0.02) \times 10^{-5}$	$(1.91 \pm 0.06) \times 10^{-5}$

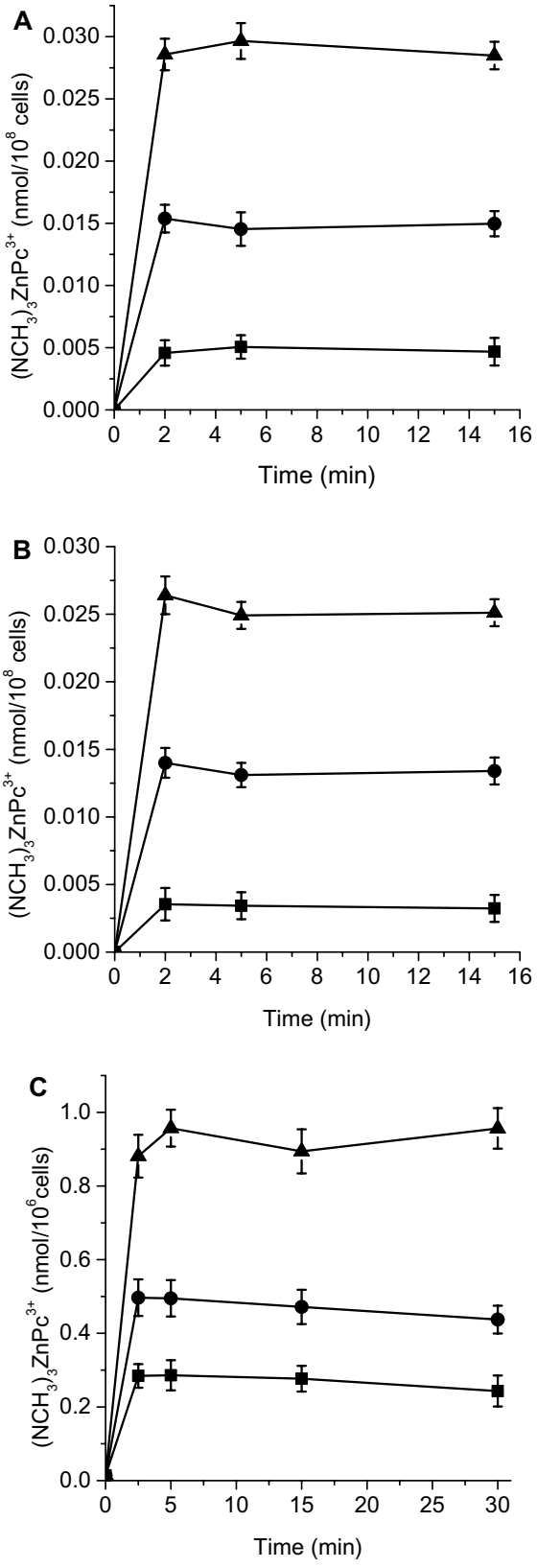

Fig. 8 Amount of $(NCH_3)_3ZnPc^{3+}$ recovered from (**A**) *S. aureus* (~10^8 CFU/mL), (**B**) *E. coli* (~10^8 CFU/mL), and (**C**) *C. albicans* (~10^6 CFU/mL) cells suspensions in PBS treated with 1.0 (filled square), 2.5 (filled circle) and 5.0 (filled triangle) μM phthalocyanine for different incubation times (2, 5, 15 and 30 min) at 37 °C in the dark

not possible to observe due to the size of the bacterial cells. Furthermore, fluorescence images were analyzed in *C. albicans* cells (Fig. 9c). Circles of red fluorescence were found in the periphery of the yeast cells, while no $(NCH_3)_3ZnPc^{3+}$ fluorescence was detected inside the cells. Similar peripheral circular red fluorescence patterns was detected in *C. albicans* cells incubated with a tricationic porphyrin (5-phenyl-10,15,20-tris(*N*-methyl-4-pyridyl)porphyrin) [52]. Therefore, the $(NCH_3)_3ZnPc^{3+}$ was mainly localized in the cell envelope of these eukaryotic cells.

3.5 Photosensitized inactivation of microorganisms

Photoinactivation of *S. aureus*, *E. coli* and *C. albicans* mediated by different concentration, 1.0 μ M, 2.5 μ M and 5.0 μ M $(NCH_3)_3ZnPc^{3+}$ and 5.0 μ M $(NCH_3)_4ZnPc^{4+}$, was investigated in PBS cell suspensions (~ 10^8 CFU/mL for bacteria and ~ 10^6 CFU/mL for *C. albicans*) after different periods of irradiations (2, 5 and 15 min for *S. aureus* and 5, 15 y 30 min for *E. coli* and *C. albicans*) with visible light (Fig. 10). The viability of the three microorganisms was unaffected by irradiation without incubation with the PS (Fig. 10). Moreover, no toxicity was found for cells incubated with phthalocyanine in the dark for 30 min (Fig. S5). Therefore, the cell mortality found after irradiation of the cultures treated with the phthalocyanine was due to the photosensitization effect of the agent induced by visible light.

As can be observed in Fig. 10, in vitro PDI investigation allowed to observe a low efficiency of $(NCH_3)_4ZnPc^{4+}$ to photoinactive microorganisms. This tetracationic phthalocyanine showed a decrease in cell viability of 3.7 log, 1.2 log and 2.8 log for *S. aureus, E. coli,* and *C. albicans*, respectively, using 5 μM PS and an irradiation time of 30 min. In contrast, $(NCH_3)_3ZnPc^{3+}$ was highly effective to photoinactivate microorganisms. A complete eradication of *S. aureus* was obtained with 1.0 μM $(NCH_3)_3ZnPc^{3+}$ and only 2 min of irradiation (Fig. 10a). Similar results were obtained in *E. coli* treated with 2.5 μM $(NCH_3)_3ZnPc^{3+}$ or in *C. albicans* incubated with 5.0 μM $(NCH_3)_3ZnPc^{3+}$ and irradiated for 5 min. The PDI results for $(NCH_3)_3ZnPc^{3+}$ revealed that the viability of *E. coli* and *C. albicans* cells was dependent on irradiation time and concentrations used in the treatment (Fig. 10b and c, respectively). An increase in the phthalocyanine concentration produced an enhancement in the PDI efficiency. Both microorganisms, *E. coli* and *C. albicans*, were rapidly photoinactivated in the presence of $(NCH_3)_3ZnPc^{3+}$.

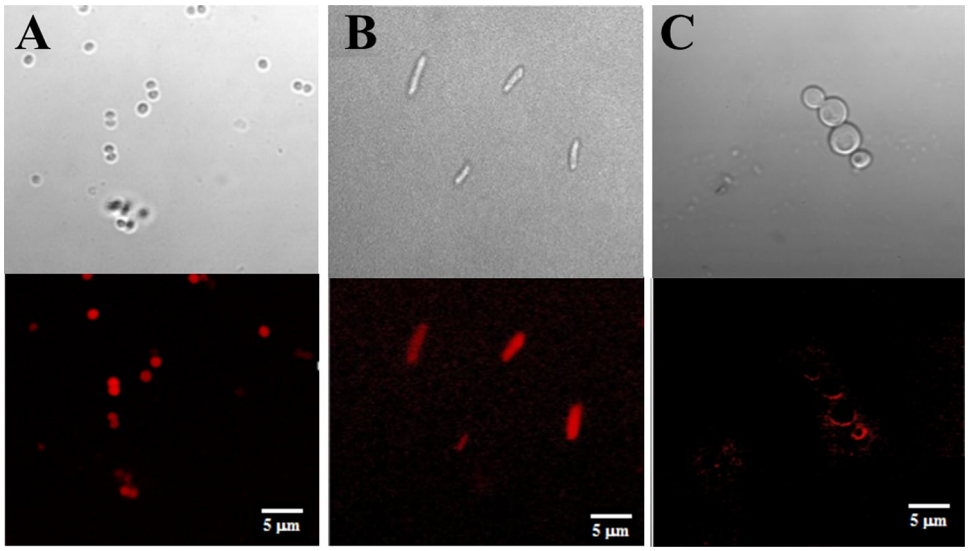

Fig. 9 Fluorescence confocal microscopic images of (**A**) *S. aureus*, (**B**) *E. coli* and (**C**) *C. albicans* incubated with 5.0 µM $(NCH_3)_3ZnPc^{3+}$ for 30 min at 37 °C in the dark (scale bar 5 µm)

This phthalocyanine produced 4.5 log decrease of *E. coli* cell survival when the cultures were incubated with 1.0 µM PS and irradiated for 5 min. The photoinactivation was similar using 2.5 and 5 µM PS producing 8 log decrease of cell survival for *E. coli* and 6 log decrease of cell survival for *C. albicans* at the same irradiation time (5 min). These results denote values greater than 99.9999% of cell photokilling. On the other hand, the photodynamic activity of $(NCH_3)_3ZnPc^{3+}$ produced an inactivation of *S. aureus* (Fig. 10a) reaching 8 log decrease in cell survival after 2 min irradiation with all concentrations used in the treatments. It was previously demonstrated that the type, number and position of the positive charges play a key role in the PDT induced by phthalocyanines against bioluminescent recombinant strain of *E. coli* [53]. Furthermore, tetracationic and amphiphilic phthalocyanines demonstrated to be efficient in the photoinactivation of microorganisms [54, 55]. Quaternized phthalocyanines proved high PDI efficiency due to the peripheral positive charges of the ammonium groups that lead to consistent electrostatic interactions with the negative groups at the cell wall of Gram-negative bacteria [56]. In the present case, for prokaryotic cells Gram-positive bacteria were more susceptible compared to Gram-negative ones to photodynamic activity sensitized by $(NCH_3)_3ZnPc^{3+}$. This difference can be attributed to the permeability barriers that surrounds these microbes. Cell wall of Gram-positive bacteria contains lipoteichoic and teichoic acids that are organized in multiple layers of peptidoglycan [57]. This envelope confers greater permeability to bacterial cells, facilitating the photodynamic action of PSs. In contrast, cell wall of Gram-negative bacteria is made up of a complex outer membrane that contains phospholipids, lipopolysaccharides, lipoteichoic acids and lipoproteins. This envelop produces a protective barrier impermeable to several antimicrobial agents. However, cationic PSs, such as $(NCH_3)_3ZnPc^{3+}$, are capable of promoting

Fig. 10 Survival curves of (**A**) *S. aureus* (~10^8 CFU/mL), (**B**) *E. coli* (~10^8 CFU/mL) and (**C**) *C. albicans* (~10^6 CFU/mL) treated with 1.0 (filled square), 2.5 (filled circle) and 5.0 (filled triangle) $(NCH_3)_3ZnPc^{3+}$ and 5.0 µM (inverted filled triangle) $(NCH_3)_4ZnPc^{4+}$ at 37 °C in the dark and exposed to visible light for different irradiation periods. Controls of cells untreated with phthalocyanine and irradiated (open circle). Values represent mean ± standard deviation of three experiments

destabilization of this membrane by electrostatic interactions, producing effective photoinactivation. On the other hand, the cell walls of eukaryotic yeast have a relatively thick layer of β-glucan and chitin that leads to a permeability barrier intermediate between Gram-positive and Gram-negative bacteria [58]. Despite this, photoinactivation of *E. coli* and *C. albicans* mediated by $(NCH_3)_3ZnPc^{3+}$ was possible even using a short irradiation period. This amphiphilic tricationic phthalocyanine was considerably more effective in inactivating yeast cells than other dicationic or tetracationic phthalocyanines, previously evaluated under similar experimental conditions [30, 32].

4 Conclusion

A novel $(NCH_3)_3ZnPc^{3+}$ phthalocyanine was synthesized by ring expansion reaction of $(NO_2)_3SubPc$ with 2,3-naphthalenedicarbonitrile, followed by reduction of nitro groups and methylation of amino substituents to obtain the three cationic substituents. This approach produced selectively a macrocycle with an A_3B-symmetry in good yield. Furthermore, a tetracationic analog $(NCH_3)_4ZnPc^{4+}$ was obtained by cyclotetramerization reaction to compare the charge distribution in phthalocyanines. The absorption and fluorescence spectra of these compounds showed the characteristic

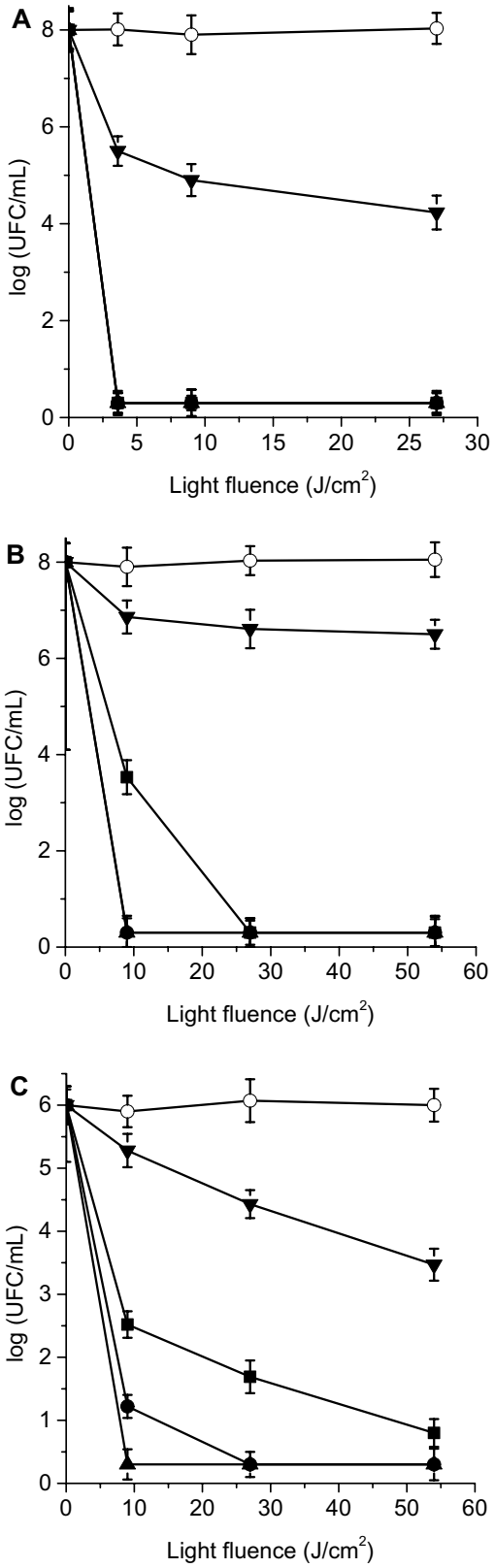

Q-bands centered at 671 nm and a maximum red emission at 677 nm, respectively. However, the ϕ_F of $(NCH_3)_4ZnPc^{4+}$ was considerably lower than that of $(NCH_3)_3ZnPc^{3+}$, possibly due to partial aggregation of tetracationic phthalocyanine. This effect also precluded the photodynamic properties of $(NCH_3)_4ZnPc^{4+}$, while $(NCH_3)_3ZnPc^{3+}$ was able to produce efficiently $O_2(^1\Delta_g)$ and $O_2^{\cdot-}$ in the presence of NADH. In addition, tricationic phthalocyanine sensitized the decomposition of Trp by means of a significant contribution of type II photoprocess. In microbial media, $(NCH_3)_3ZnPc^{3+}$ was rapidly uptake by cells in times as short as 2 min. After short irradiation periods, this compound was effective to eliminate *S. aureus*, *E. coli* and *C. albicans*. Therefore, the amphiphilic tricationic $(NCH_3)_3ZnPc^{3+}$ is an interesting antimicrobial phototherapeutic with possible biomedical applications to eradicate microorganisms.

Supplementary Information The online version contains supplementary material available at https://doi.org/10.1007/s43630-021-00074-2.

Acknowledgements This work was supported by UNRC-SECYT (PPI-2020 Res. 083/20) and ANPCYT (PICT 0667/16). J.E.D., N.S.G., M.E.M. and E.N.D. are Scientific Members of CONICET. E.B. thanks CONICET for the research fellowship.

Declarations

Conflict of interest There are no conflicts to declare.

References

1. Lee, J., Perera, D., Glickman, T., & Taing, L. (2020). Water-related disasters and their health impacts: A global review. *Progress in Disaster Science, 8*, 100123.
2. Rass, E., Lokot, M., Brown, F. L., Fuhr, D. C., Asmar, M. K., Smith, J., McKee, M., Orm, I. B., Yeretzian, J. S., & Roberts, B. (2020). Participation by conflict-affected and forcibly displaced communities in humanitarian healthcare responses: A systematic review. *Journal of Migration and Health, 1–2*, 100026.
3. Hiller, C. X., Hubner, U., Fajnorova, S., Schwartz, T., & Drewes, J. E. (2019). Antibiotic microbial resistance (AMR) removal efficiencies by conventional and advanced wastewater treatment processes: A review. *Science of the Total Environment, 685*, 596–608.
4. Lee, V. C. (2015). The antibiotic resistance crisis part 1: Causes and threats. *Pharmacology & Therapeutics, 40*, 277–283.
5. Klein, E. Y., Van Boeckel, T. P., Martinez, E. M., Pant, S., Gandra, S., Levin, S. A., Goossens, H., & Laxminarayan, R. (2018). Global increase and geographic convergence in antibiotic consumption between 2000 and 2015. *Proceedings of the National Academy of Sciences, 115*, 3463–3470.
6. Fernandez, P., & Martens, E. (2017). Antibiotics in late clinical development. *Biochemical Pharmacology, 133*, 152–163.
7. Theuretzbacher, U. (2013). Review global antibacterial resistance: The never-ending story. *Journal of Global Antimicrobial Resistance, 1*, 63–69.
8. Kashef, N., & Hamblin, M. R. (2017). Can microbial cells develop resistance to oxidative stress in antimicrobial photodynamic inactivation? *Drug Resistance Updates, 31*, 31–42.
9. Durantini, A. M., Heredia, D. A., Durantini, J. E., & Durantini, E. N. (2018). BODIPYs to the rescue: Potential applications in photodynamic inactivation. *European Journal of Medicinal Chemistry, 144*, 651–661.

10. Wang, Y.-Y., Liu, Y.-C., Sun, H., & Guo, D.-S. (2019). Type I photodynamic therapy by organic–inorganic hybrid materials: From strategies to applications. *Coordination Chemistry Reviews, 395*, 46–62.
11. Di Mascio, P., Martinez, G. R., Miyamoto, S., Ronsein, G. E., Madeiros, M. H. G., & Cadet, J. (2019). Singlet molecular oxygen reactions with nucleic acids, lipids, and proteins. *Chemical Reviews, 119*, 2043–2086.
12. Bolla, J.-M., Alibert-Franco, S., Handzlik, J., Chevalier, J., Mahamoud, A., Boyer, G., Kieć-Kononowicz, K., & Pagès, J.-M. (2011). Strategies for bypassing the membrane barrier in multidrug resistant Gram-negative bacteria. *FEBS Letters, 585*, 1682–1690.
13. Lo, P.-C., Salomé Rodríguez-Morgade, M., Pandey, R. K., Ng, D. K. P., Torres, T., & Dumoulin, F. (2020). The unique features and promises of phthalocyanines as advanced photosensitisers for photodynamic therapy of cancer. *Chemical Society Reviews, 49*, 1041–1056.
14. Dumoulin, F., Durmus, M., Ahsen, V., & Nyokong, T. (2010). Synthetic pathways to water-soluble phthalocyanines and close analogs. *Coordination Chemistry Reviews, 254*, 2792–2847.
15. Wong, R. C. H., Lo, P.-C., & Ng, D. K. P. (2019). Stimuli responsive phthalocyanine-based fluorescent probes and photosensitizers. *Coordination Chemistry Reviews, 379*, 30–46.
16. Li, X., Zheng, B.-D., Peng, X.-H., Li, S.-Z., Ying, J.-W., Zhao, Y., Huang, J.-D., & Yoon, J. (2019). Phthalocyanines as medicinal photosensitizers: Developments in the last five years. *Coordination Chemistry Reviews, 379*, 147–160.
17. Olofsson, M., Matussek, A., Ehricht, R., Lindgren, P.-E., & Östgren, C. J. (2019). Differences in molecular epidemiology of *Staphylococcus aureus* and *Escherichia coli* in nursing home residents and people in unassisted living situations. *Journal of Hospital Infection, 101*, 76–83.
18. Janbon, G., Quintin, J., Lanternier, F., & d'Enfert, C. (2019). Studying fungal pathogens of humans and fungal infections: Fungal diversity and diversity of approaches. *Microbes and Infection, 21*, 237–245.
19. Sastre, A., Torres, T., Díaz-García, M. A., Agulló-López, F., Dhenaut, C., Brasselet, S., Ledoux, I., & Zyss, J. (1996). Subphthalocyanines: Novel targets for remarkable second-order optical nonlinearties. *Journal of the American Chemical Society, 118*, 2746–2747.
20. Chauhan, S. M. S., & Kumari, P. (2009). Synthesis of unsymmetrical benzoporphyrazines in functional ionic liquids and formation of self-aggregates of zinc(II) pyridino[3,4]tribenzoporphyrazines in solutions. *Tetrahedron, 65*, 2518–2524.
21. Cong, F.-D., Ning, B., Du, X.-G., Ma, C.-Y., Yu, H.-F., & Chen, B. (2005). Facile synthesis, characterization and property comparisons of tetraaminometallophthylocyanines with and without intramolecular hydrogen bonds. *Dyes and Pigments, 66*, 149–154.
22. Miretti, M., Clementi, R., Tempesti, T. C., & Baumgartner, M. T. (2017). Photodynamic inactivation of multiresistant bacteria (KPC) using zinc(II) phthalocyanines. *Bioorganic & Medicinal Chemistry Letters, 27*, 4341–4344.
23. Agazzi, M. L., Durantini, J. E., Gsponer, N. S., Durantini, A. M., Bertolotti, S. G., & Durantini, E. N. (2019). Light-harvesting antenna and proton-activated photodynamic effect of a novel BODIPY-fullerene C_{60} dyad as potential antimicrobial agent. *ChemPhysChem, 20*, 1110–1125.
24. Hanwell, M. D., Curtis, D. E., Lonie, D. C., Vandermeersch, T., Zurek, E., & Hutchison, G. R. (2012). Avogadro: An advanced semantic chemical editor, visualization, and analysis platform. *Journal of Cheminformatics, 4*, 1–7.
25. Scalise, I., & Durantini, E. N. (2005). Synthesis, properties, and photodynamic inactivation of *Escherichia coli* using a cationic and a noncharged Zn(II) pyridyloxyphthalocyanine derivatives. *Bioorganic & Medicinal Chemistry, 13*, 3037–3045.
26. Ochoa, A. L., Tempesti, T., Spesia, M. B., Milanesio, M. E., & Durantini, E. N. (2012). Synthesis and photodynamic properties of adamantylethoxy Zn(II) phthalocyanine derivatives in different media and in human red blood cells. *European Journal of Medicinal Chemistry, 50*, 280–287.
27. Yslas, E. I., Rivarola, V., & Durantini, E. N. (2005). Synthesis and photodynamic activity of zinc(II) phthalocyanine derivatives bearing methoxy and trifluoromethylbenzyloxy substituents in homogeneous and biological media. *Bioorganic & Medicinal Chemistry, 13*, 39–46.
28. Ferreyra, D. D., Reynoso, E., Cordero, P., Spesia, M. B., Alvarez, M. G., Milanesio, M. E., & Durantini, E. N. (2016). Synthesis and properties of 5,10,15,20-tetrakis[4-(3-N, N-dimethylaminopropoxy)phenyl] chlorin as potential broad-spectrum antimicrobial photosensitizers. *Journal of Photochemistry and Photobiology B: Biology, 158*, 243–251.
29. Scanone, A. C., Gsponer, N. S., Alvarez, M. G., & Durantini, E. N. (2018). Porphyrins containing basic aliphatic amino groups as potential broadspectrum antimicrobial agents. *Photodiagnosis and Photodynamic Therapy, 24*, 220–227.
30. Di Palma, M. A., Alvarez, M. G., Ochoa, A. L., Milanesio, M. E., & Durantini, E. N. (2013). Optimization of cellular uptake of zinc(II) 2,9,16,23-tetrakis[4-(*N*-methylpyridyloxy)]phthalocyanine for maximal photoinactivation of *Candida albicans*. *Fungal Biology, 117*, 744–751.
31. Ballatore, M. B., Milanesio, M. E., Fujita, H., Lindsey, J. S., & Durantini, E. N. (2020). Bacteriochlorin-bis(spermine) conjugate affords an effective photodynamic action to eradicate microorganisms. *Journal of Biophotonics, 13*, e201960061.
32. Tempesti, T. C., Alvarez, M. G., & Durantini, E. N. (2011). Synthesis and photodynamic properties of amphiphilic A_3B-phthalocyanine derivatives bearing *N*-heterocycles as potential cationic phototherapeutic agents. *Dyes and Pigments, 91*, 6–12.
33. Wang, A., Long, L., & Zhang, C. (2012). Synthesis of unsymmetrical phthalocyanines: A brief overview. *Tetrahedron, 68*, 2433–2451.
34. Claessens, C. G., González-Rodríguez, D., Rodríguez-Morgade, M. S., Medina, A., & Torres, T. (2013). Subphthalocyanines, subporphyrazines, and subporphyrins: Singular nonplanar aromatic systems. *Chemical Reviews, 114*, 2192–2277.
35. Yılmaz, Y., Mack, J., Şener, M. K., Sönmez, M., & Nyokong, T. (2014). Photophysical and photochemical properties and TD-DFT calculations of novel zinc and platinum phthalocyanines. *Journal of Photochemistry and Photobiology A: Chemistry, 277*, 102–110.
36. Kostka, M., Zimcik, P., Miletin, M., Klemera, P., Kopecky, K., & Musil, Z. (2006). Comparison of aggregation properties and photodynamic activity of phthalocyanines and azaphthalocyanines. *Journal of Photochemistry and Photobiology A: Chemistry, 178*, 16–25.
37. Suchetti, C. A., & Durantini, E. N. (2007). Monomerization and photodynamic activity of Zn(II) tetraalkyltetrapyridinoporphyrazinium derivatives in AOT reverse micelles. *Dyes and Pigments, 74*, 630–635.
38. Ogunsipe, A., & Nyokong, T. (2004). Effects of substituents and solvents on the photochemical properties of zinc phthalocyanine complexes and their protonated derivatives. *Journal of Molecular Structure, 689*, 89–97.
39. Luc, N.-Q., Dang, V.-S., Tran, Q.-T., Pham, V.-T., & Mai, A.-T. (2020). Density Function Theory calculation, and phthalonitrile process for a synthesis of single crystal zinc phthalocyanine. *Materials Science in Semiconductor Processing, 113*, 105025.

40. Dupouy, E. A., Lazzeri, D., & Durantini, E. N. (2004). Photodynamic activity of cationic and non-charged Zn(II) tetrapyridinoporphyrazine derivatives: Biological consequences in human erythrocytes and *Escherichia coli*. *Photochemical & Photobiological Sciences, 3*, 992–998.
41. Cormick, M. P., Rovera, M., & Durantini, E. N. (2008). Synthesis, spectroscopic properties and photodynamic activity of a novel Zn(II) phthalocyanine substituted by fluconazole groups. *Journal of Photochemistry and Photobiology A: Chemistry, 194*, 220–229.
42. Yamakoshi, Y., Umezawa, N., Ryu, A., Arakane, K., Miyata, N., Goda, Y., Masumizu, T., & Nagano, T. (2003). Active oxygen species generated from photoexcited fullerene (C_{60}) as potential medicines: $O_2^{\cdot-}$ versus $^1O_2$. *Journal of the American Chemical Society, 125*, 12803–12809.
43. Ballatore, M. B., Spesia, M. B., Milanesio, M. E., & Durantini, E. N. (2018). Mechanistic insight into the photodynamic effect mediated by porphyrin-fullerene C_{60} dyads in solution and in *Staphylococcus aureus* cells. *RSC Advances, 8*, 22876–22886.
44. Gsponer, N. S., Agazzi, M. L., Spesia, M. B., & Durantini, E. N. (2016). Approaches to unravel pathways of reactive oxygen species in the photoinactivation of bacteria induced by a dicationic fulleropyrrolidinium derivative. *Methods, 109*, 167–174.
45. Tavares, A., Dias, S. R. S., Carvalho, C. M. B., Faustino, M. A. F., Tomé, J. P. C., Neves, M. G. P. M. S., Tomé, A. C., Cavaleiro, J. A. S., Cunha, Â., Gomes, N. C. M., Alves, E., & Almeida, A. (2011). Mechanisms of photodynamic inactivation of a Gram-negative recombinant bioluminescent bacterium by cationic porphyrins. *Photochemical & Photobiological Sciences, 10*, 1659–1669.
46. Lebedeva, N. S., Yurina, E. S., Gubarev, Y. A., Lyubimtsev, A. V., & Syrbu, S. A. (2018). Effect of irradiation spectral range on porphyrin-protein complexes. *Journal of Photochemistry and Photobiology A: Chemistry, 353*, 299–305.
47. Ehrensha, M., Deterding, L. J., & Mason, R. P. (2015). Tripping up Trp: Modification of protein tryptophan residues by reactive oxygen species, modes of detection, and biological consequences. *Free Radical Biology and Medicine, 89*, 220–228.
48. Baigorria, E., Milanesio, M. E., & Durantini, E. N. (2020). Synthesis, spectroscopic properties and photodynamic activity of Zn(II)phthalocyanine-polymer conjugates as antimicrobial agents. *European Polymer Journal, 134*, 109816.
49. Milanesio, M. E., Alvarez, M. G., Rivarola, V., Silber, J. J., & Durantini, E. N. (2005). Porphyrin-fullerene C_{60} dyads with high ability to form photoinduced charge-separated state as novel sensitizers for photodynamic therapy. *Photochemistry and Photobiology, 84*, 891–897.
50. da Silva, E. F. F., Pedersen, B. W., Breitenbach, T., Toftegaard, R., Kuimova, M. K., Arnaut, L. G., & Ogilby, P. R. (2012). Irradiation- and sensitizer-dependent changes in the lifetime of intracellular singlet oxygen produced in a photosensitized process. *The Journal of Physical Chemistry B, 116*, 445–461.
51. Maisch, T., Bosl, C., Szeimies, R.-M., Lehn, N., & Abels, C. (2005). Photodynamic effects of novel XF porphyrin derivatives on prokaryotic and eukaryotic cells. *Antimicrobial Agents and Chemotherapy, 49*, 1542–1552.
52. Lambrechts, S. A. G., Aalders, M. C. G., & Van Marle, J. (2005). Mechanistic study of the photodynamic inactivation of *Candida albicans* by a cationic porphyrin. *Antimicrobial Agents and Chemotherapy, 49*, 2026–2034.
53. Lourenço, L. M. O., Sousa, A., Gomes, M. C., Faustino, M. A. F., Almeida, A., Silva, A. M. S., Neves, M. G. P. M. S., Cavaleiro, J. A. S., Cunha, Â., & Tomé, J. P. C. (2015). Inverted methoxypyridinium phthalocyanines for PDI of pathogenic bacteria. *Photochemical & Photobiological Sciences, 14*, 1853–1863.
54. Sindelo, A., Kobayashi, N., Kimura, M., & Nyokong, T. (2019). Physicochemical and photodynamic antimicrobial chemotherapy activity of morpholine-substituted phthalocyanines: Effect of point of substitution and central metal. *Journal of Photochemistry & Photobiology A: Chemistry, 374*, 58–67.
55. Revuelta-Maza, M. A., González-Jiménez, P., Hally, C., Agut, M., Nonell, S., de la Torre, G., & Torres, T. (2020). Fluorine-substituted tetracationic ABAB-phthalocyanines for efficient photodynamic inactivation of Gram-positive and Gram-negative bacteria. *European Journal of Medicinal Chemistry, 187*, 111957.
56. Lourenço, L. M. O., Rocha, D. M. G. C., Ramos, C. I. V., Gomes, M. C., Almeida, A., Faustino, M. A. F., Almeida Paz, F. A., Neves, M. G. P. M. S., Cunha, Â., & Tomé, J. P. C. (2019). Photoinactivation of planktonic and biofilm forms of *Escherichia coli* through the action of cationic zinc(II) phthalocyanines. *ChemPhotoChem, 3*, 251–260.
57. Malanovic, N., & Lohner, K. (2016). Gram-positive bacterial cell envelopes: The impact on the activity of antimicrobial peptides. *Biochimica et Biophysica Acta Biomembranes, 1858*, 936–946.
58. Dai, T., Huanga, Y.-Y., & Hamblin, M. R. (2009). Photodynamic therapy for localized infections-state of the art. *Photodiagnosis and Photodynamic Therapy, 6*, 170–188.